CHAPTER VII

DESCRIPTION OF THE HYDRODYNAMIC MODEL AND SIMULATION

7.1 Introduction

In this study, a transient, two dimensional multiphase computer code for the solution of generalization of Navier-Stokes equations developed earlier for gas-liquid-solids fluidization was verified. The particulate viscosities are either an input into the code or are obtained from fluctuating energy equations derived from the Boltzmann equation for velocity distribution of particles. Previously, a number of investigators have studied and simulated gas-solids bubbling fluidized beds (Seo and Gidaspow, 1987; Gidaspow and Ettehadieh, 1983) and gas-liquid fluidized beds (Gidaspow et al., 1991). The emerging kinetic theory of granular flow (Jenkins and Savage, 1983; Lun et al., 1984) shows how to predict stresses caused by particle collisions. Ding and Gidaspow (1990) applied this theory to gas-solids fluidized beds. A review of modeling of the hydrodynamics of fluidization of bubbling beds by Gidaspow (1986) showed that inviscid two-fluid models were able to predict a great deal of the behavior of bubbling beds because the dominant mechanism of energy dissipation is the drag between the particles and the fluid. The formation, growth and bursting of bubbles were predicted. Predicted wall-to-bed heat transfer coefficients and velocity profiles of jets agreed with measurements.

Although the partial differential equations that we are solving are well-posed as

an initial value problem, a problem of how to prescribe inlet conditions for the gas phase needs to be understood. This problem arises due to the asymmetric circulation of gas, liquid and solids inside the bed. The asymmetric inlet conditions for gas phase give us experimentally observed bubble coalescence and velocity distributions in the three-phase fluidized bed which were not seen for a symmetric bed.

7.2 Hydrodynamic Model

The physical principles used are the laws of conservation of mass and momentum for the gas, the liquid and the solid phases as shown in Table D.1 in Appendix D. The constitutive equation for the stress is also shown in Table D.1 in Appendix D. This approach is similar to that of Soo (1967) for multiphase flow and of Jackson (1985) for fluidization. The equations are similar to Bowen's (1976) balance laws for multicomponent mixtures. The principle difference is the appearance of the volume fraction of phase "k" denoted by ε_k. In the case of phases, not all the space is occupied at the same time by all the phases, as it is by components. As in the case of the mixture equations for components, the mixture equations for phases show that the sum of the drag forces is zero. The fluid pressure p_l is in the liquid (continuous) phase.

The corresponding gas and solids (dispersed particulate phases) momentum equations with zero particulate viscosities are the trajectory equations for particulate flow. For gas-solid fluidized beds, Bouillard, et al. (1989) have shown that this set of equations produces essentially the same numerical answers for fluidization as did the earlier conditionally stable model which has the fluid pressure in both the gas and the solids

phases. In this model (hydrodynamic model B) the drag and the stress relations were altered to satisfy Archimedes' buoyancy principle and Darcy's law, as illustrated by Jayaswal (1991). The gas-particulate drag coefficients given in Table D.1 are for the model B reviewed by Jayaswal (1991). For the solid phase, p_s consists of the static normal stress and the dynamic stress, called solids pressure, which arises due to the collision of the particles. The added mass forces, Saffman's lift forces (Birkoff, 1960; Saffman, 1965; Drew, et al., 1979) were assumed to be negligible.

This model is unconditionally well-posed, i.e., the characteristics are real and distinct for one dimensional transient flow. It does not require the presence of solids pressure for stability and well posedness.

The details of hydrodynamic equations used in the computer simulation are given in Table D.1 of the Appendix D.

7.3 Numerical Scheme

The governing equations along with the constitutive equations are solved for p_l, ε_k, u_k and v_k, (k = g, l, s) using the Implicit Continuum Eulerian (ICE) method (Rivard and Torrey, 1977; Jayaswal, 1991) with appropriate initial and boundary conditions. The pressure drop was assumed to be in liquid (continuous) phase. Stewart and Wendroff (1984) have critically reviewed the ICE algorithm and related staggered mesh conservative schemes. The computations are carried out using a mesh of finite-difference cells fixed in two-dimensional space (Eulerian mesh). The scaler variables are located at the cell center and the vector variables at the cell boundaries. The momentum equation

is solved using staggered mesh whereas for the continuity equation the donor cell method was used.

The partial differential equations are well-posed. The time step is chosen to satisfy the Courant stability criterion (Courant, et al., 1952). The numerical stability of the equations can be obtained using the von Neumann stability analysis, as illustrated by Lyczkowski, et al. (1978) and Prosperetti (1982).

7.4. Initial and Boundary Conditions

As an initial condition, the liquid-solid bed was assumed to be at a minimum fluidization state. The gas and liquid flows at the bottom of the bed were started at specified rates at time t = 0. No-slip condition was satisfied at the wall.

The computer simulations of the three-phase fluidized bed were carried out in two different modes described later : symmetric and asymmetric. A complete inlet and initial conditions for both the modes are shown in Figure 7.1. In both the modes, simulations were carried out for 20 seconds with a time increment of 5×10^{-5} seconds. The computations were conducted on our HP-700 workstation.

7.5 Fluidized Bed Simulation

7.5.1 Symmetric Fluidized Bed Mode. In symmetric mode, the fluidized bed behavior was assumed to be symmetric across the centerline parallel to the axial direction. In this mode only half of the bed was simulated. The computations were carried out using a mesh of 1040 finite difference computational cells with 0.635 cm x 2 cm cell

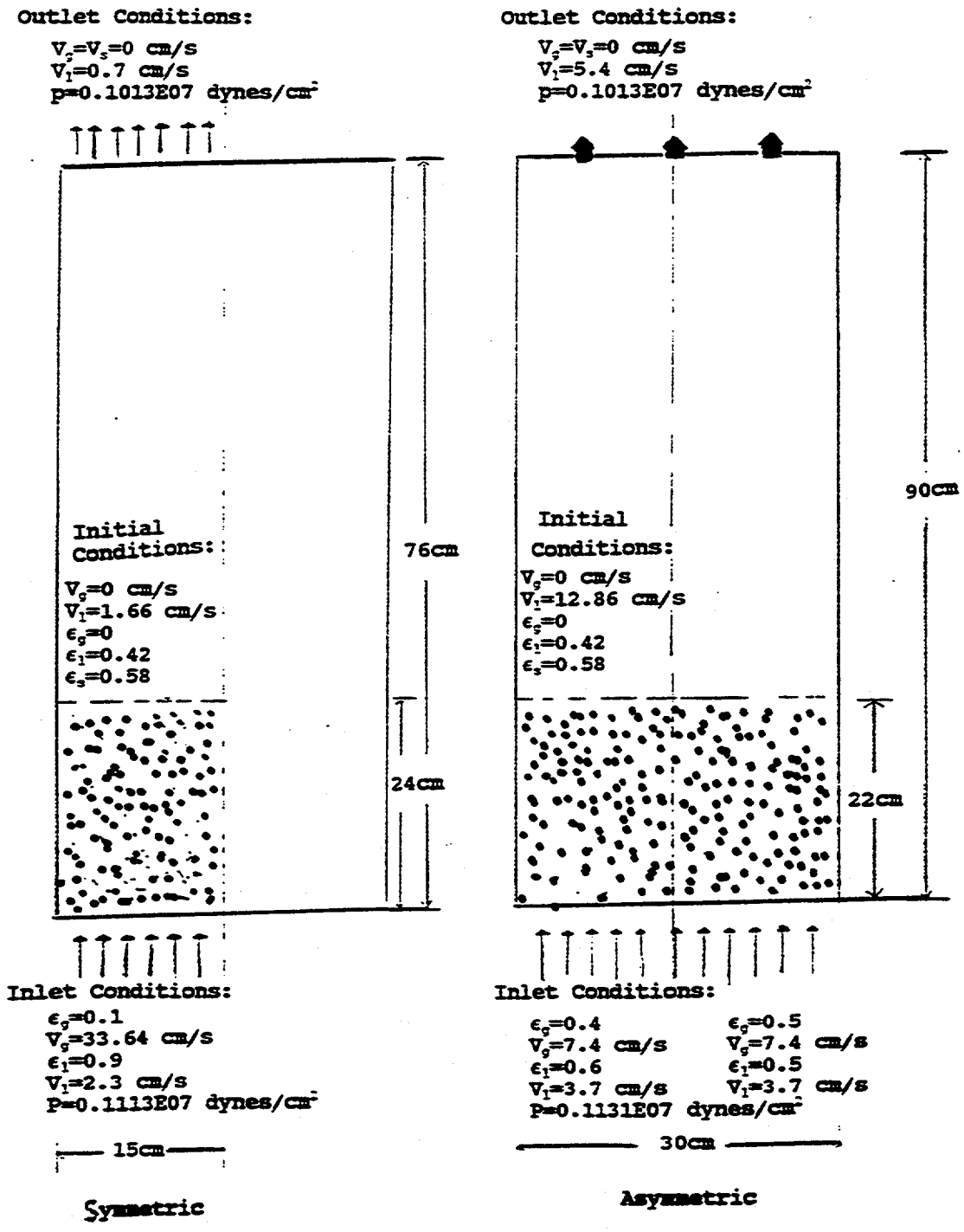

Figure 7.1. System for Simulation of Three Phase Fluidized Bed with Dimensions and Flow Conditions

sizes.

7.5.2 Asymmetric Fluidized Bed Mode. In asymmetric mode, it was assumed that the gas at the inlet entering the two sides of the bed had different volume fractions. This assumption is also supported by the visual observation of the experiment. In this mode, the complete bed was simulated. A total of 1504 computational cells with 1.016 cm x 2 cm cell sizes were used. The simulation in this mode was done in two different types of fluidized beds :

a) One-outlet bed : bed with completely open outlet at the top.

b) Multi-outlet bed: In this setup, the geometry was modified to include the multiple outlets of the bed in order to closely match the experimental set-up. The fluidized bed had three 1.0 inch x 1.0 inch (2.54 cm x 2.54 cm) rectangular equispaced openings at the top of the bed.

7.6 Results of Numerical Simulation

Numerical computations, using the hydrodynamic model presented in Table D.1, were carried out for the three-phase fluidized bed. Typical results of the simulation are presented below.

7.6.1 Volume Fraction Profiles. The computed time-averaged volume fraction contours for gas, liquid and solids in the two dimensional fluidized bed are shown in Figures 7.2(a) to 7.2(c), respectively.

The computed volume fractions of gas and liquid near the wall compare well with measurements; which were found to be approximately 0.3 for gas and 0.5 for liquid.

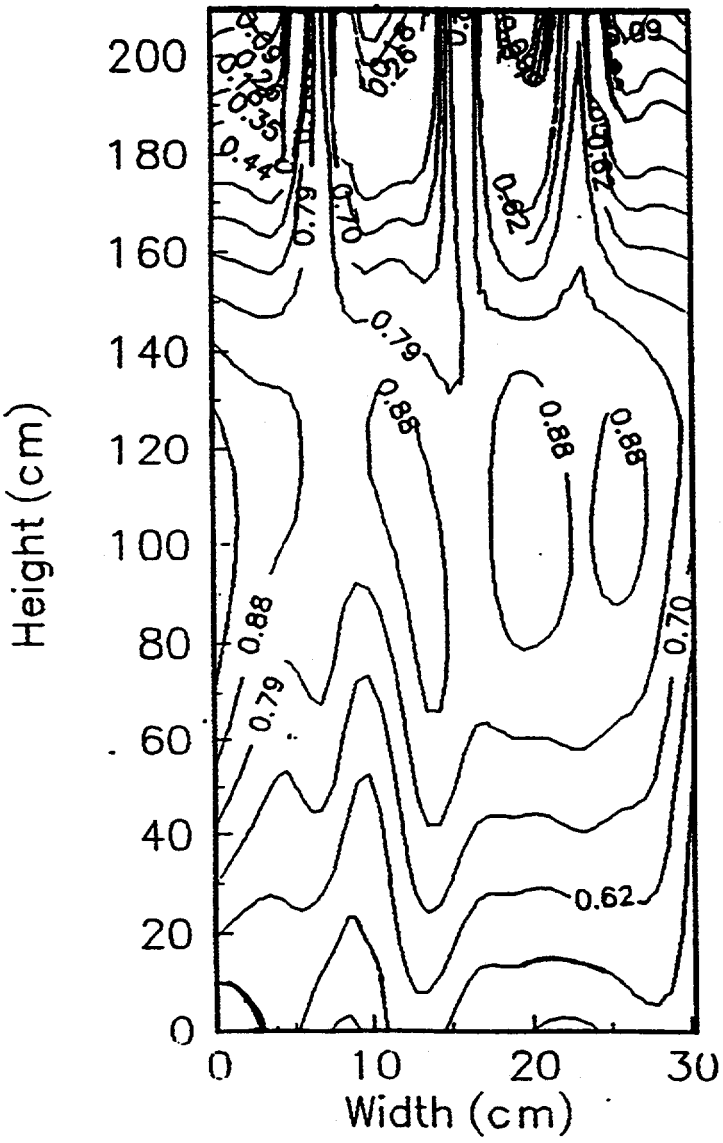

Figure 7.2(a). Computed Time Average Volume Fraction Contours for Liquid Phase

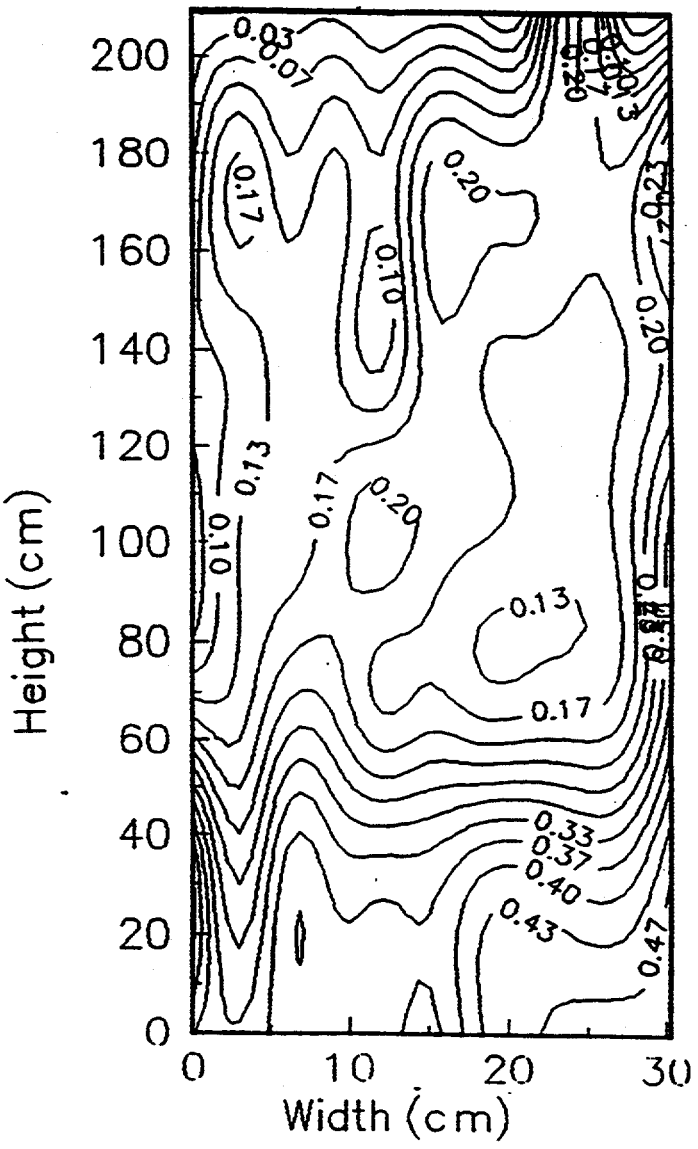

Figure 7.2(b). Computed Time Average Volume Fraction Contours for Gas Phase

Figure 7.2(d). Photograph of Bubble Coalescence in a Liquid-Gas-Solid Fluidized Bed (U_g=3.37 cm/sec, U_l=2.03 cm/sec)

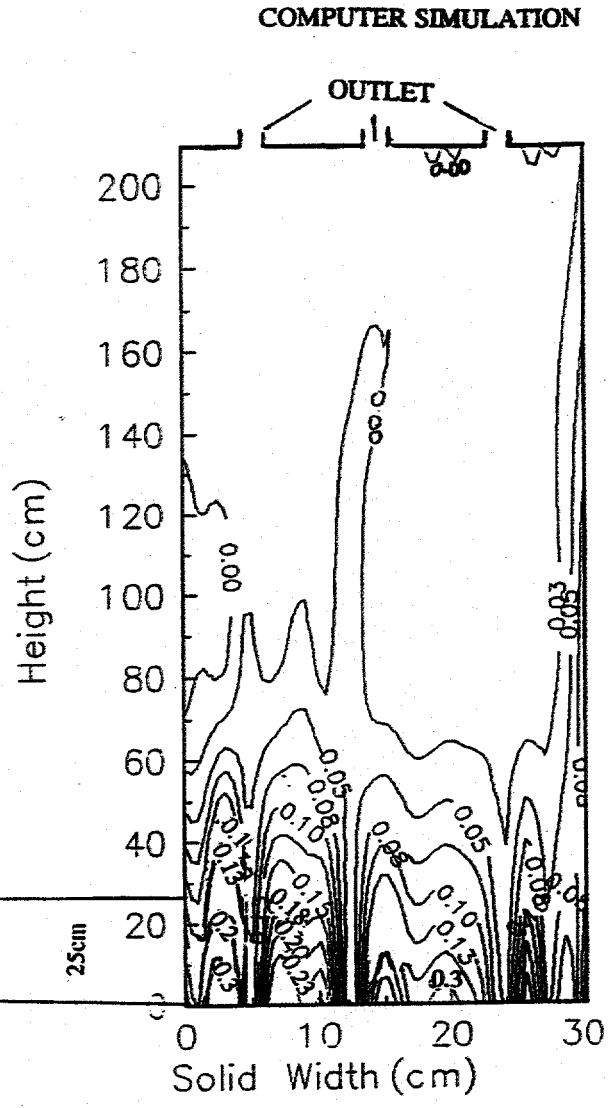

Figure 7.2(c). Computed Time Average Volume Fraction Contours for Solid Phase

Computed time averaged solid volume fraction contours for the whole bed with three outflows are shown in Figures 7.2(c), as in the photograph of the experiment, Figure 7.2(d) shows that the solid is concentrated in the lower 25 cm of the bed. There is a murky interface between the solid and the liquid-gas in the upper portion of the bed. This is in part reality and in part caused by perhaps inadequate time averaging. We time averaged over about 20 seconds. Higher time averaging can not be used due to a small loss of particles observed both in the experiment and more so in the simulation. The simulation has larger particles loss due to the neglect of the walls in the two dimensional computations. To correct this deficiency we are in the process of developing a three dimensional code.

Figure 7.2(b) shows that there is more gas in the lower portion of the bed than in the region where there is only gas and liquid. Figures 7.3 to 7.5 demonstrate a comparison between the computed and measured time-average volume fractions of three phases at different widths of the bed. In most cases, near the wall and the center, there is good agreement between the computational and experimental results.

Figures 7.6 and 7.7 show computations for instantaneous gas volume fractions in the form of bubbles for symmetric and asymmetric cases, respectively. In both cases, symmetric and asymmetric, we see a tendency for gas bubbles to move midway between the center of the bed and the walls. In the symmetric case of the three-phase fluidized bed, no bubble coalescence was observed. The reason for no bubble coalescence is the downward flow in the center of the bed causing a deficiency of gas in that region. In asymmetric case, however, shows bubble coalescence.

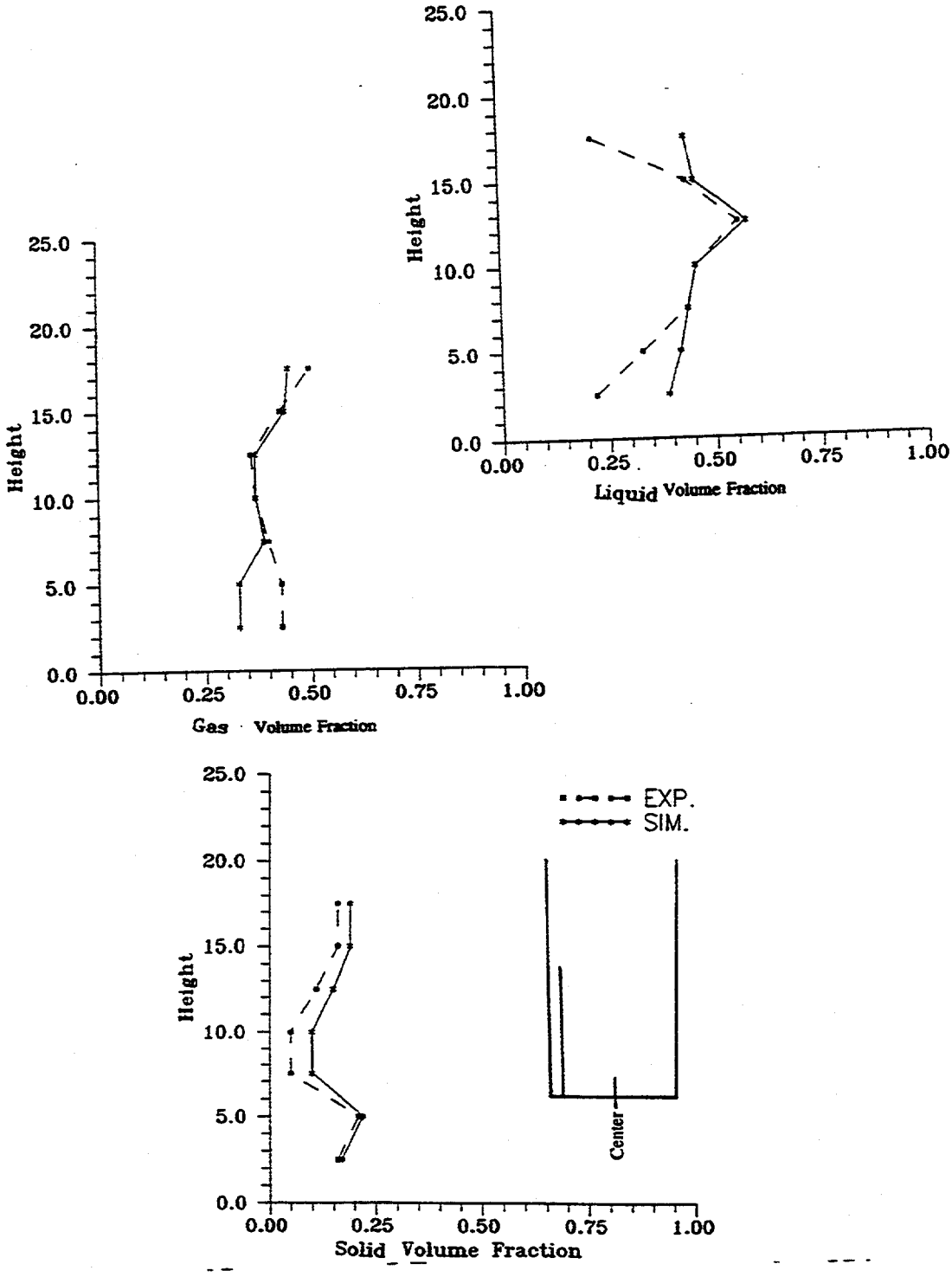

Figure 7.3. Comparison of Computational and Experimental Time Average Volume Fractions at X=2.0 cm

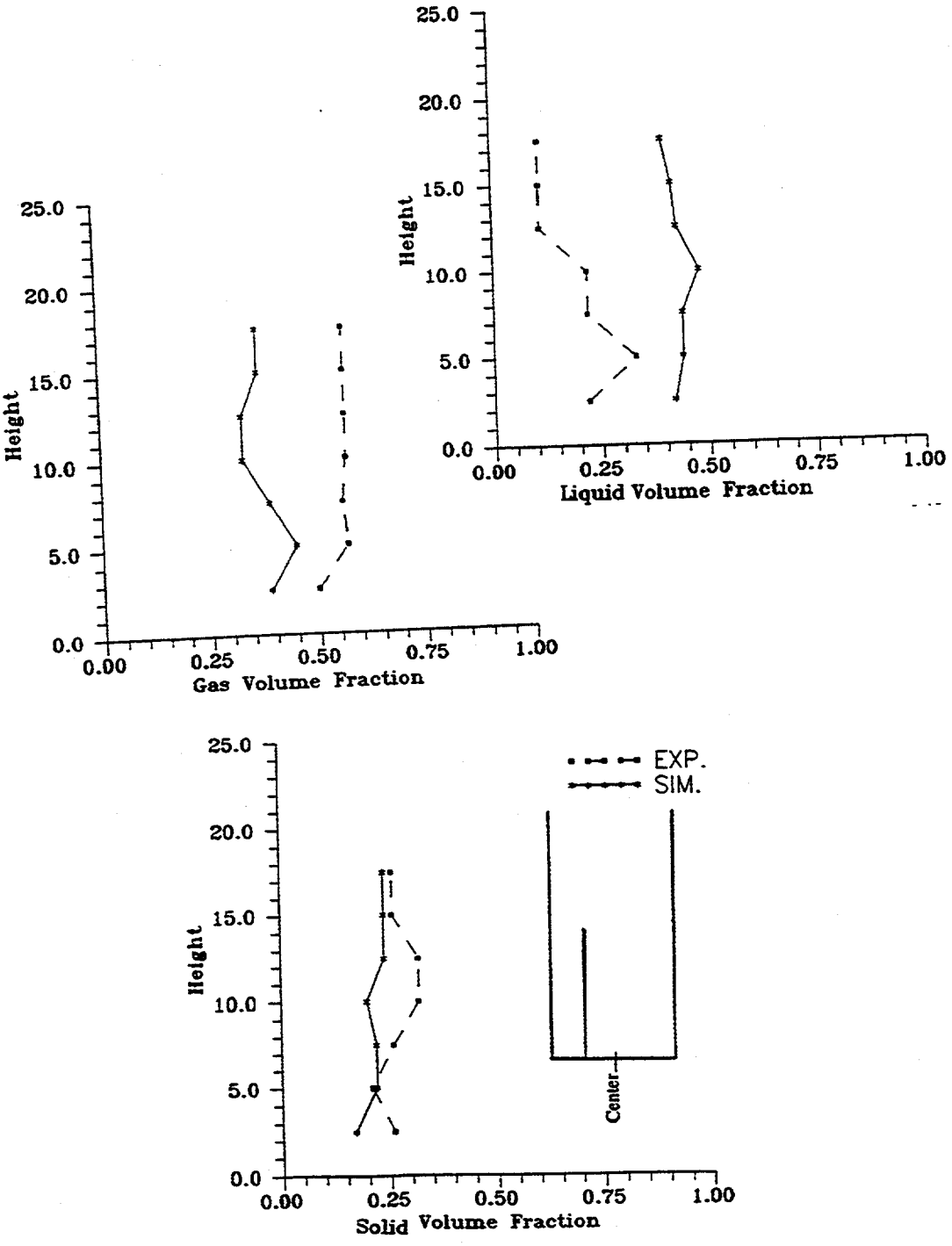

Figure 7.4. Comparison of Computational and Experimental Time Average Volume Fractions at X=7.0 cm

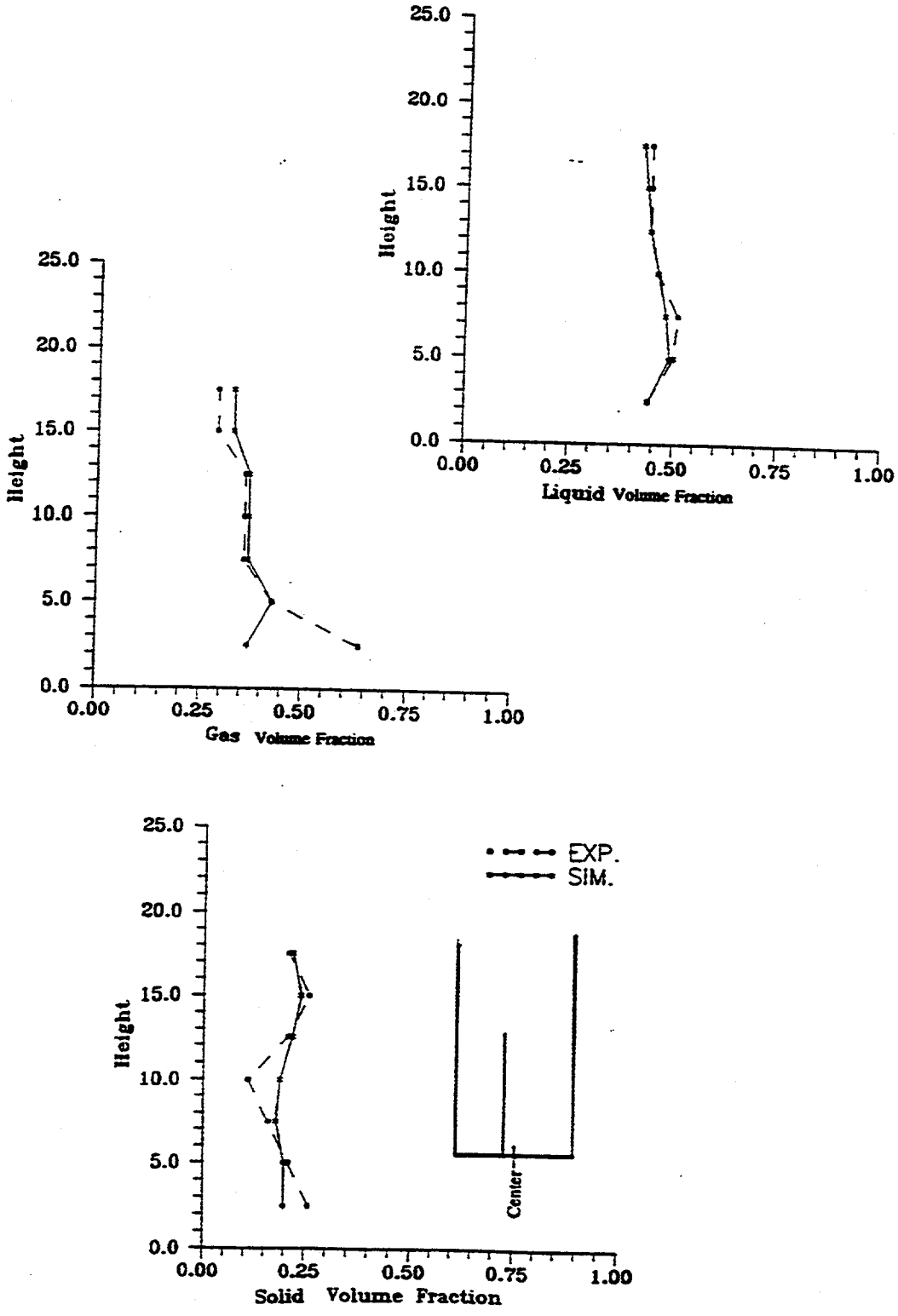

Figure 7.5. Comparison of Computational and Experimental Time Average Volume Fractions at X=11.0 cm

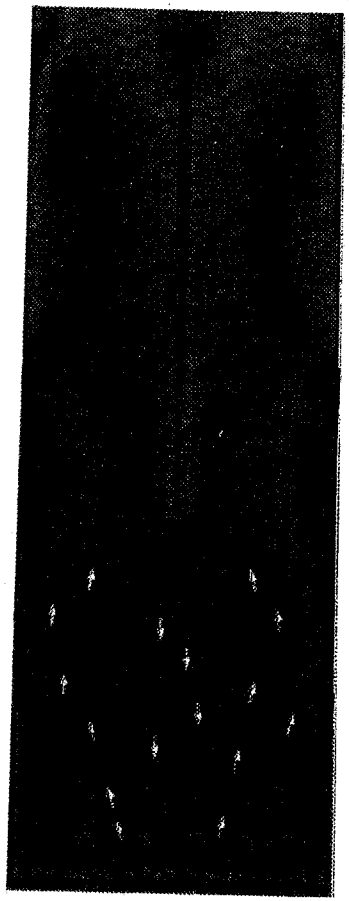

Figure 7.6. Bubble Formation in Three Phase Fluidized Bed at Time = 1.5 sec, for Symmetric Bed

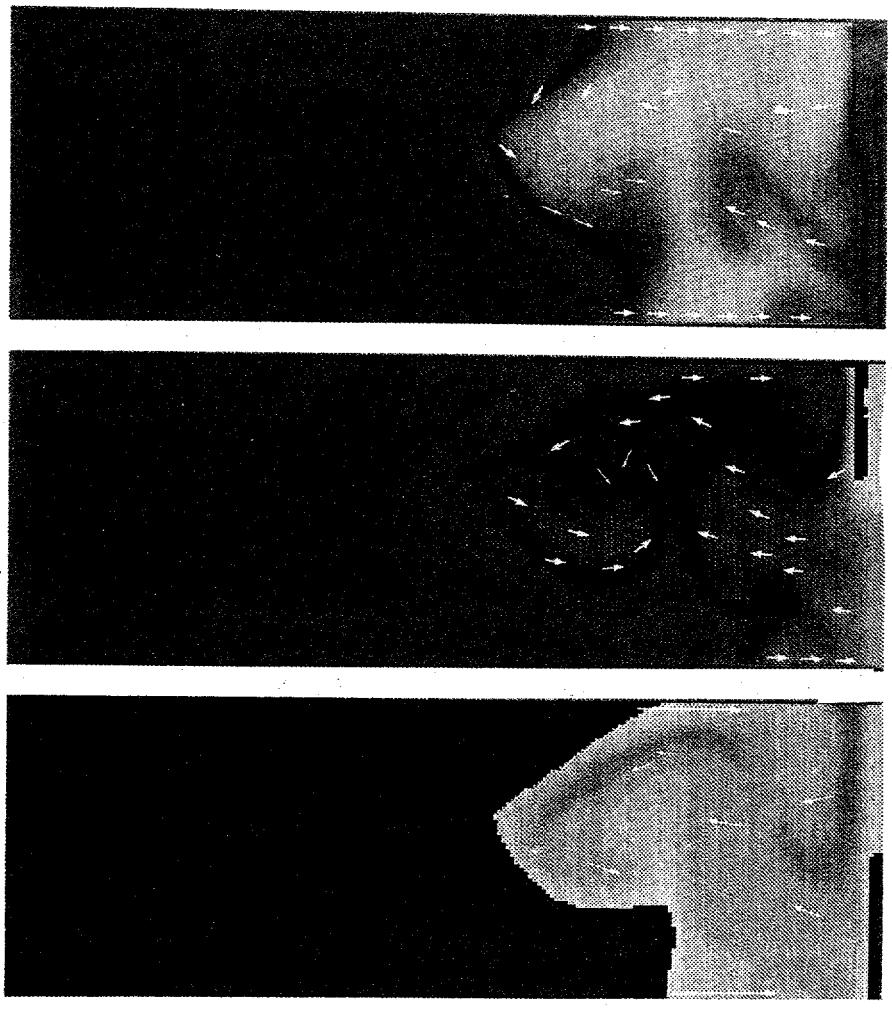

Figure 7.7. Bubble Formation in Three Phase Fluidized Bed at Time = 2 Sec, for Asymmetric Bed

The asymmetric mode, the computed gas bubbles move in snake-like fashion as observed in the experiment. This mode is setup by vorticities generated by gas flow circulation which produces an asymmetric gas volume fraction gradient inside the fluidized bed. The computed viscosity is very high in the region of the large bubbles.

These results clearly show the need for computer simulation to be in asymmetric mode to get experimentally observed bed behavior.

7.6.2 Velocity Profiles. Figures 7.8 and 7.9 show the velocity patterns in asymmetric and symmetric cases, respectively. From these figures it is clear that in the symmetric cases, all three phases have downward movement at the center of the bed and at the wall. However, in the asymmetric mode all three phases have downward movement near the wall and upward movement at the center, the same flow pattern reported by Chen, Reese, and Fan (1994). The experimentally observed flow circulation is the same as that obtained in the asymmetric case.

The downflow seen in asymmetric mode produces a rotation or particle vorticity, given by the inviscid equation below,

$$\frac{\partial \zeta}{\partial t} + u\frac{\partial \zeta}{\partial x} + v\frac{\partial \zeta}{\partial y} = -\frac{g}{(1-\epsilon_{mf})}\frac{\partial \epsilon}{\partial y} \qquad (7.1)$$

The equation shows that the vorticity produces a change in gas volume fraction ϵ. Then although we supply gas at an uniform rate, the gas is no longer uniformly distributed. Furthermore, Bouillard and Gidaspow (1991) have shown that when the gas at the bottom moves faster than in the rest of the bed, there is a catch-up effect and large gas voids may form, as depicted by Figure 7.2(d). It is the packing effect of the bubbles

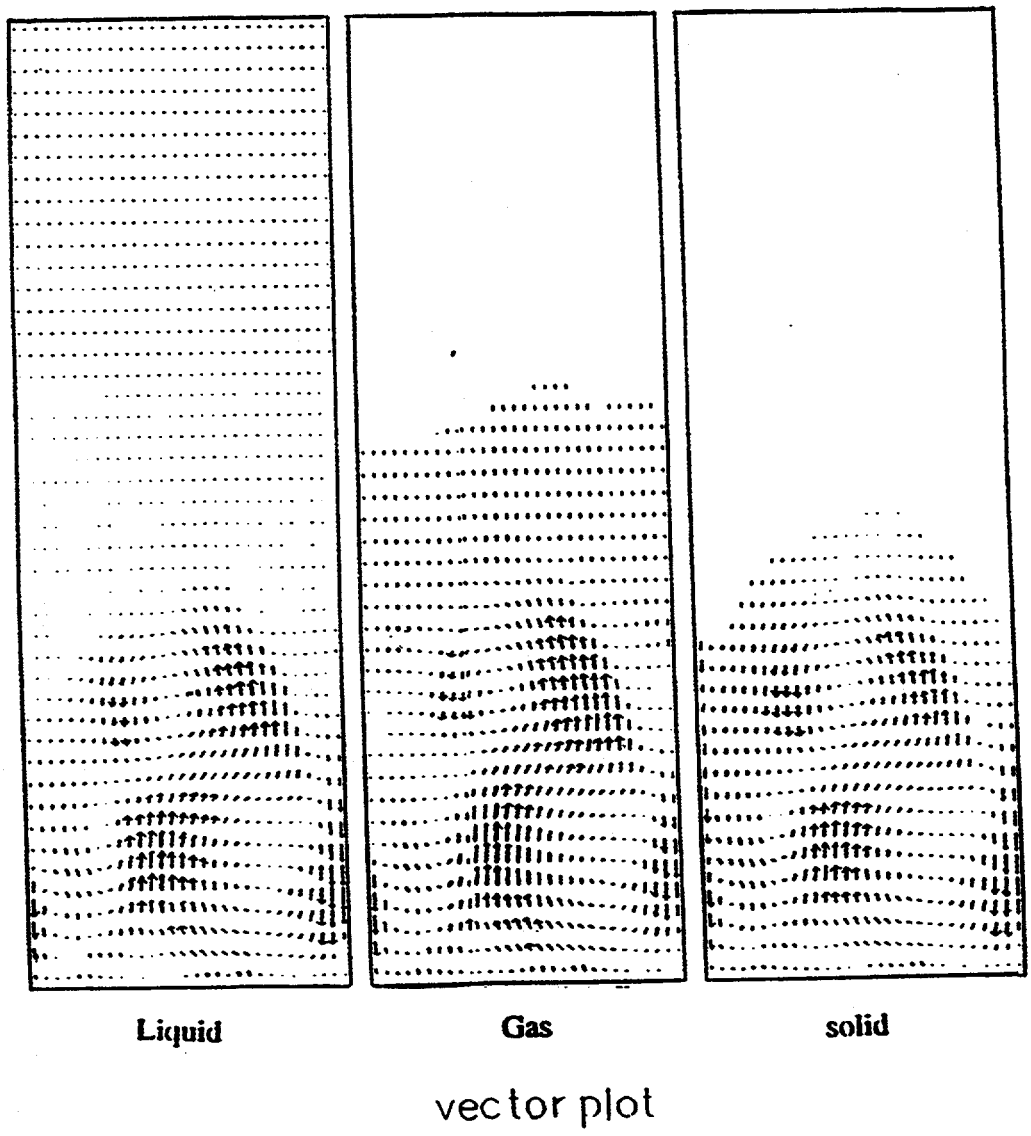

Figure 7.8. Computed Velocity Pattern in Three Phase Fluidized Bed at Time = 2 sec for Asymmetric Bed

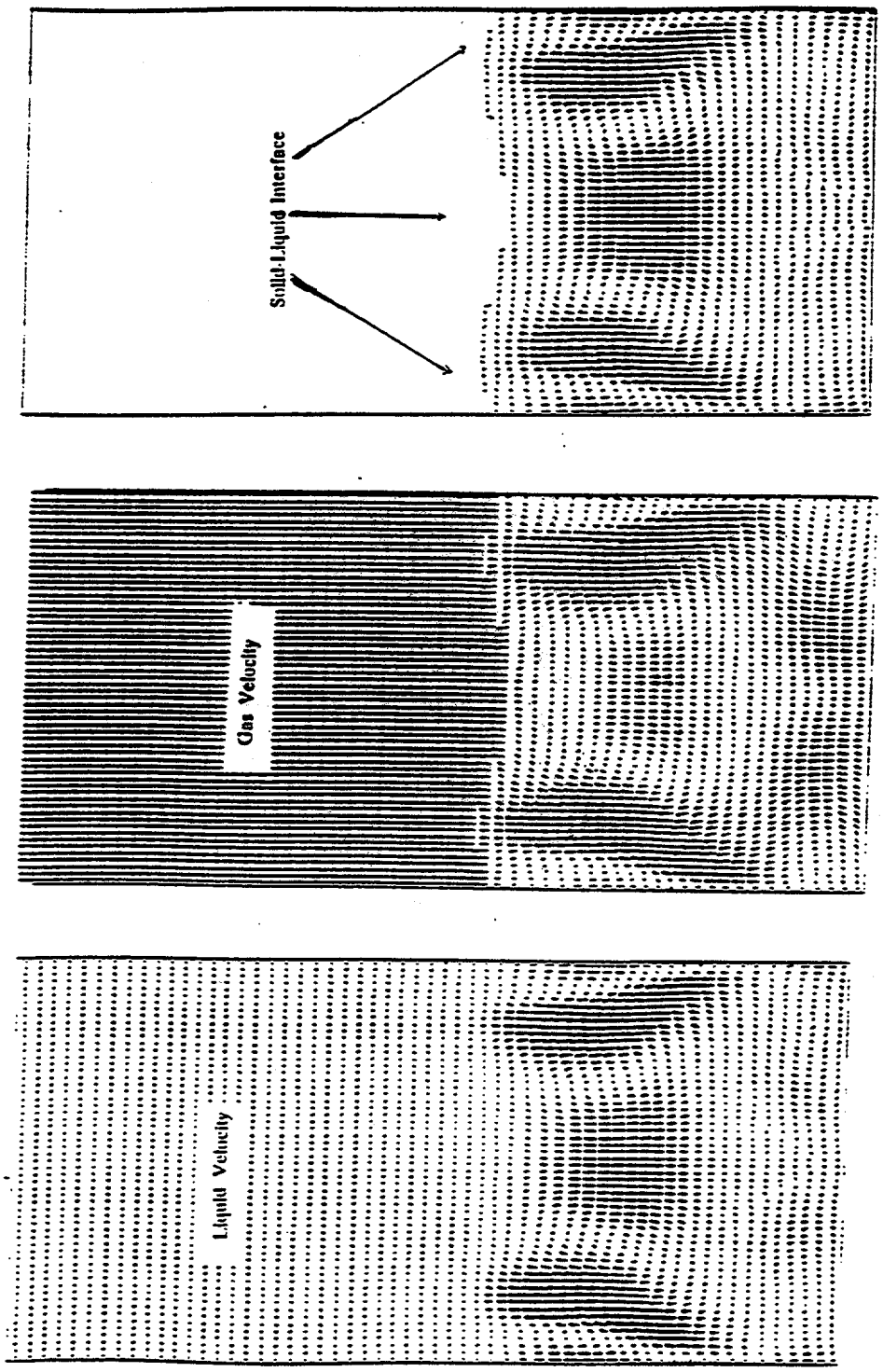

Figure 7.9. Computed Velocity Pattern in Three Phase Fluidized Bed at Time = 2 sec for Symmetric Bed

that produces this regime. When the injected bubbles are far apart, for low gas velocities, the bubbles move up at constant velocities. In this regime the drag is independent of the gas volume fraction. It is given by the corrected Stoke's law. At high gas velocities, the gas volume fraction is high and we use the Ergun equation to compute the drag in our model. Here the paths of the small injected bubbles intersect and bubbles coalesce. The situation is similar to that described in Chapter 6 for gas-solid fluidized beds by Gidaspow (1994).

Figures 7.10 and 7.11 show comparisons of time-averaged axial solids velocity profiles at heights of 7.0 cm and 13.0 cm from the bottom of the bed. These figures show excellent similarity. In Figure 7.10, there is slight disagreement between experimental and simulation velocity profiles. This disagreement mainly resulted from the positions of two liquid inlets in the bottom of the bed. In spite of a large pressure drop (about 10-20% of bed pressure drop through the liquid distributor) residual inlet effects could be seen on high experimental solids axial velocities. The residual velocity effect, however, was absent in velocity measurements conducted at a height of 13.0 cm, as seen in Figure 7.11.

7.7 Conclusion

1. Unlike gas-solid bubbling fluidized beds, the three-phase fluidized bed primarily behaves in an asymmetric fashion. The three-phase fluidized bed simulations in asymmetric mode showed promising results. Good agreement was obtained between measured and simulated solids volume fractions.

2. The asymmetric simulation also captured some characteristics of bubble coalescence and break-up. A coalesced bubbling regime was used in the experiments.

3. Excellent comparison was seen between measured and simulated time averaged solids axial velocity profiles at two different locations in the bed.

4. The multi-phase hydrodynamic model was validated for use in three-phase fluidized bed simulation.

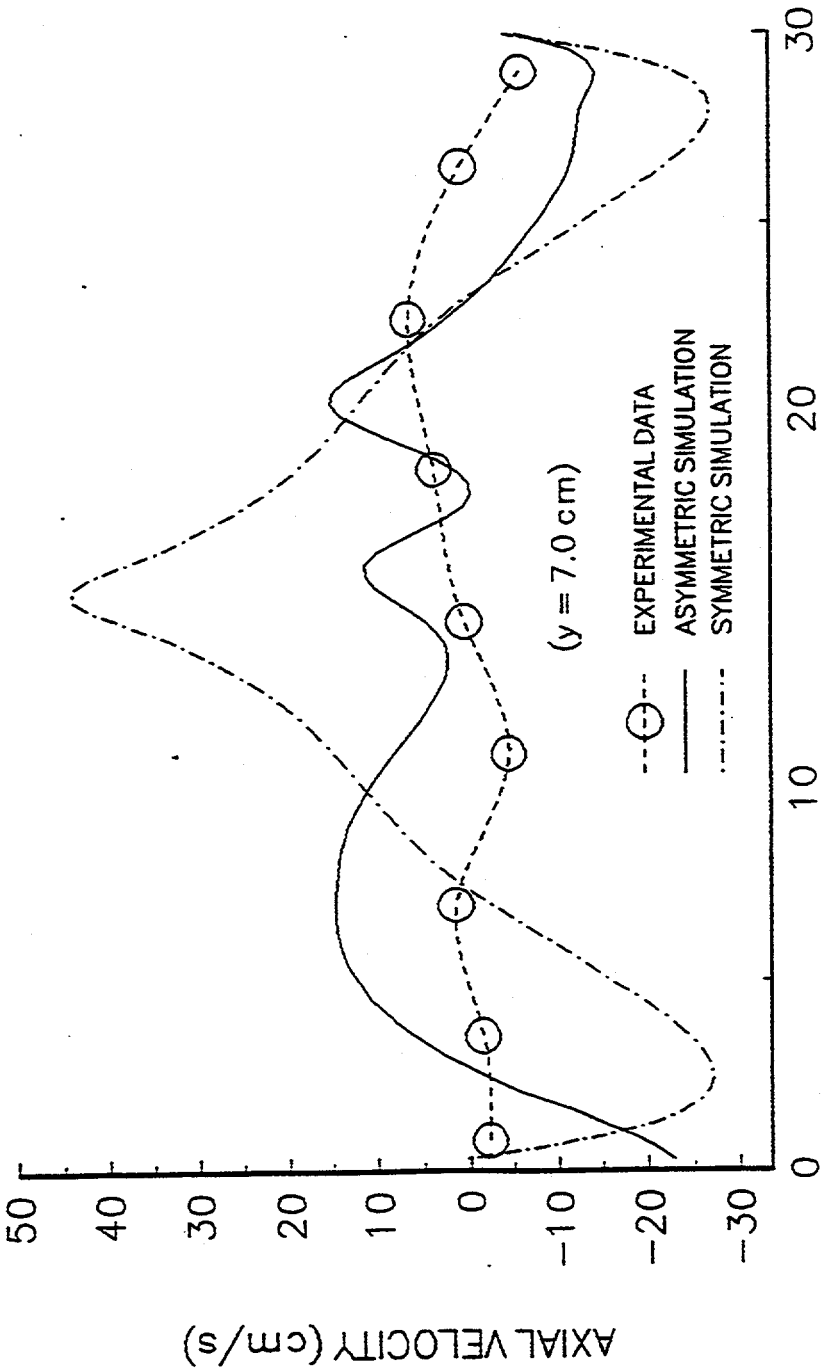

Figure 7.10. Comparison of Experimental and Computational Results for Solid Velocity Profile at Y=7 cm

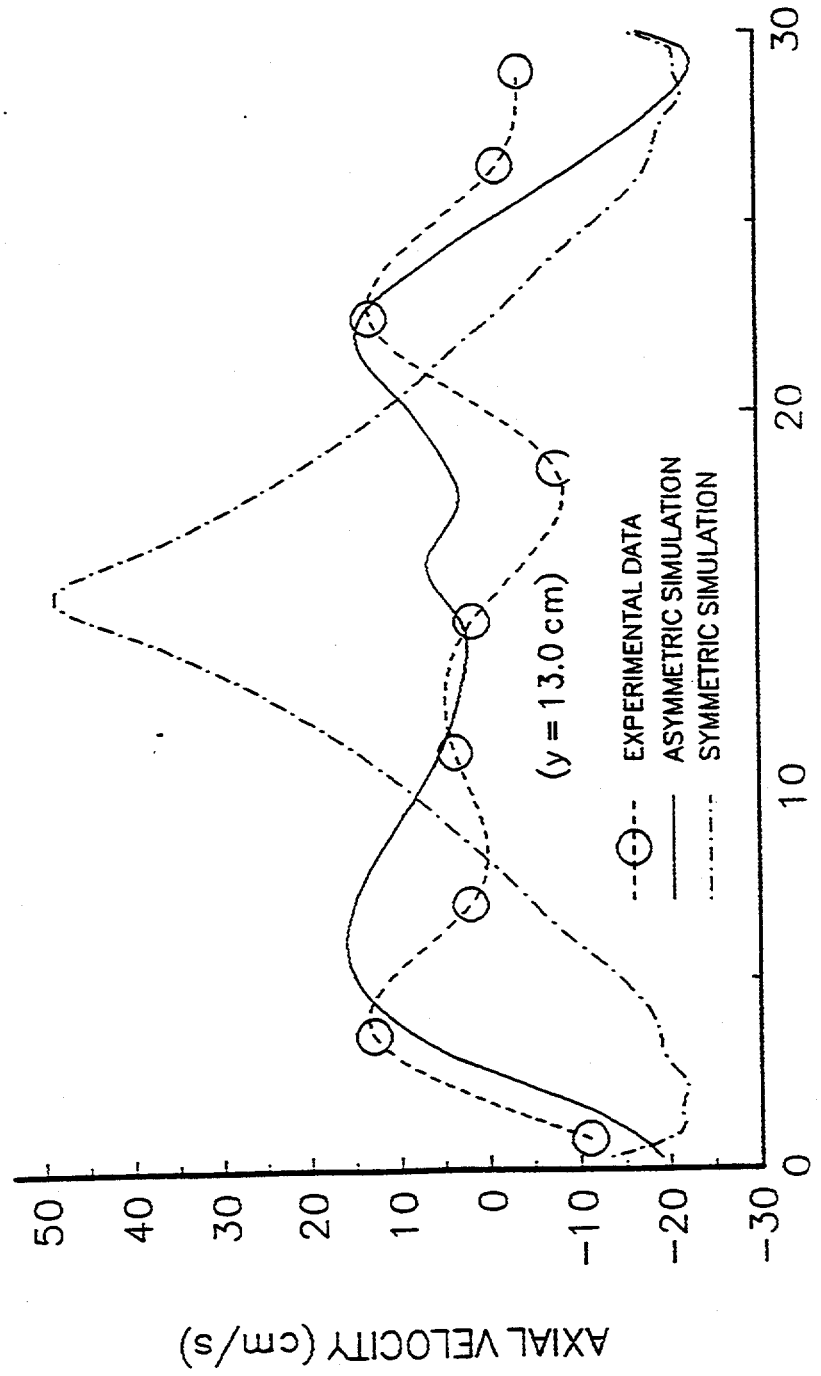

Figure 7.11. Comparison of Experimental and Computational Results for Solid Velocity Profile at Y=13 cm